

Diffraction

– Crystalline & Disorder Structures

Chun Loong, CNAIST, U. Rome Tor Vergata

ckloong@gmail.com



30 April-9 May, 2014 ENCSC-Erice

Please call me Chun & remember ckloong@gmail.com

I want my lectures to be interrupted by questions;

Any question – my answer may be “I don’t know...but let’s examine it further by...”

PPT slides without detailed narrative are often of little use;

I do have a set of write-up (Word files) supplementary to the lectures. Will be delighted to give it to you if you *ask or write me an email*.

Take-home notions you should have towards the neutron science & methodology;

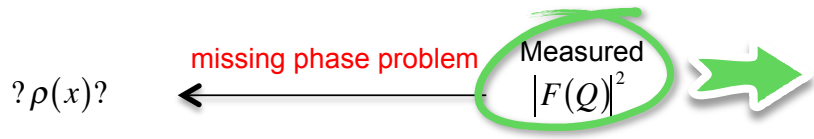
1. INTERESTED
2. IMPRESSED
3. INSPIRED
4. INNOVATIVE

What if you fail?

.....TOO BAD! You should repeat the school

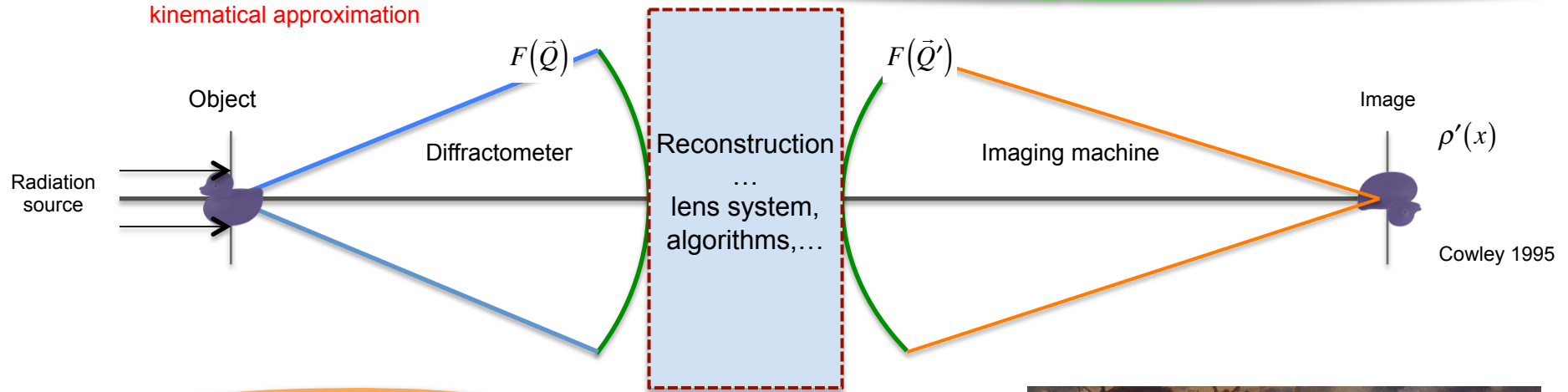
I DECLEAR MY FAILURE NOW BECAUSE I WANT TO BE BACK TO ERICE!!

A big picture unifying diffraction and imaging



- ✧ Crystalline materials - chemical & magnetic
 - ✧ Disordered structures
 - ✧ Large structures - SANS
- See also lectures by Roger Pynn & Ian Anderson

$\rho(\vec{r}) \sim \int d\vec{r}' F(\vec{Q}) \exp(-i\vec{Q} \cdot \vec{r})$
kinematical approximation



Cowley 1995

Coherent Diffraction Imaging

Presently achievable:
Synchrotron x-rays & Electrons

- Neutron microscopy
- Neutron holography



Very cold neutrons:
Source Coherency?
Instrumentation?
Methodology?

From images to discoveries?



Image of an ancient shaman's hand, 25-10,000 years ago



Cro-Magnon: Prehistoric human history

The phase problem & at the outset of a proposal

The missing phase in diffraction experiments prohibits the resolution of a structure by direct inverse Fourier transform. In principle, there are a number of ways to deal with the problem, such as by including the anomalous scattering and other dynamical-diffraction effects, or by imposing additional constraints. (e.g., the direct method). But, for neutron diffraction, most of these treatments are not effective. In practice, derivation of crystal structures relies mainly on a goodness-of-fit method of the intensity against a structural model.

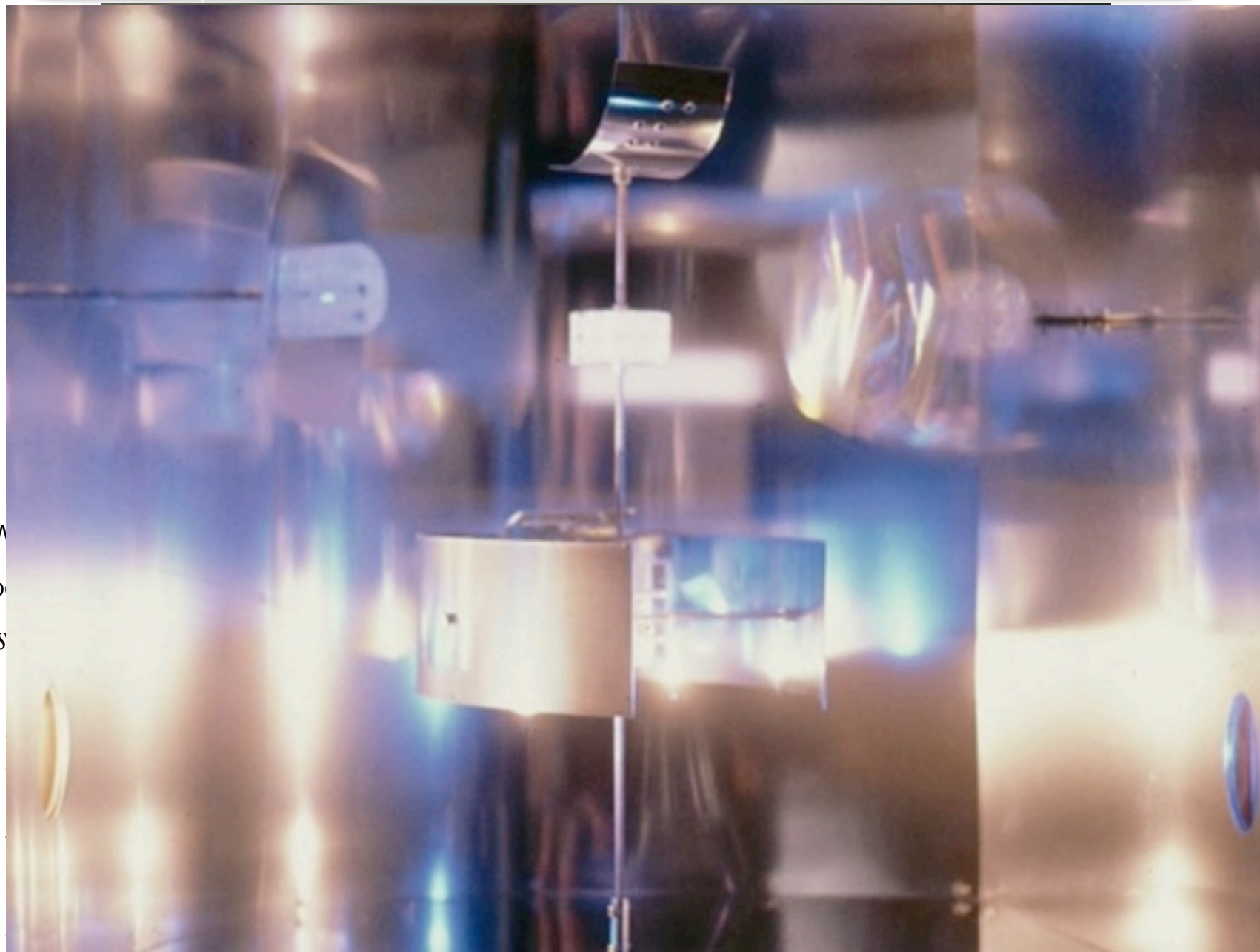
Suppose you write a proposal like...

“We have synthesized a new material that has enormous impact on modern technological and economic development... or “We have discovered a historic relic that holds the secrets of human history and civilization... but we have absolutely no knowledge of the atomic structure of this substance. Therefore we propose a neutron diffraction study of the structure.....”

Unfortunately, this proposal will likely be rejected because solving an unknown structure from scratch by neutron diffraction is impractical—too expensive and there are better characterization techniques to achieve a preliminary structure (e.g., x-ray diffraction). One should do this first before using neutrons. Furthermore, one should articulate the neutron data analysis method for extracting unique information and the big picture of fulfilling the requirements for a complete, outstanding study.

Complementary techniques & Collaborative motif of a project

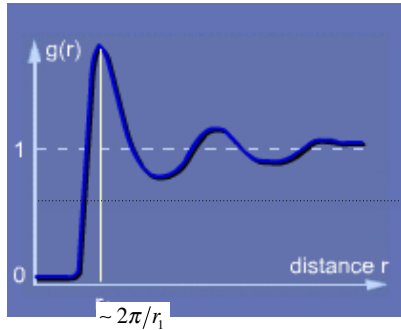
Diffraction aims at the determination of the 'average' structure of a many-body system.



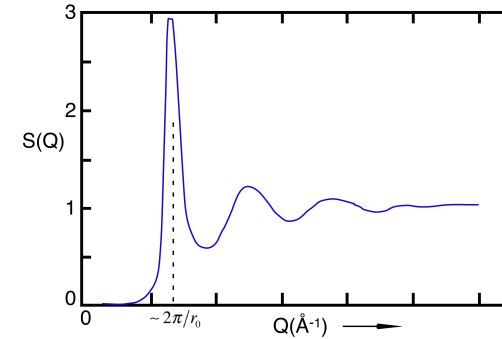
W
b
S

Q: Can one infer a qualitative structure by looking at a measured $S(Q)$?

A: No, not without some detailed analysis or modeling.



$$2\pi^2 r \rho_0 [g(r) - 1] = \int_0^\infty Q [S(Q) - 1] \sin(Qr) dQ.$$

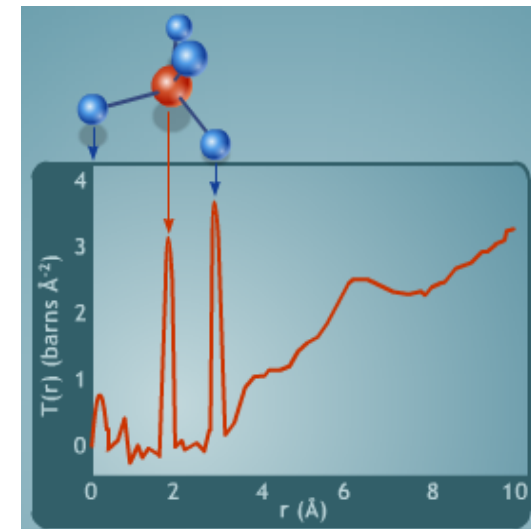


We define $G(r)$, the **total correlation function $T(r)$** and the **radial distribution function $N(r)$** in real space in terms of the measured structure factor:

$$G(r) = \frac{1}{2\pi^2 \rho_0} \int_0^\infty Q^2 [S(Q) - 1] \frac{\sin Qr}{Qr} dQ$$

$$T(r) = 4\pi r \rho_0 G(r), \text{ and } N(r) = 4\pi r^2 \rho_0 G(r)$$

The peaks in $T(r)$ represent the most probable (average) bond distances for various combinations of elements. The area under a peak of $N(r)$ corresponds to the coordination number between two atoms



Q: How about incoherent elastic scattering?

A: Incoherent scattering reveals no relative positions among atoms. But it may provide information about the confinement of a single atom, e.g., hydrogen atoms in a molecular solution.

As for the incoherent elastic scattering cross section,

$$\begin{aligned} \left(\frac{d\sigma}{d\Omega} \right)_{inc}^{el} &= (b_{inc})^2 I_s(\vec{Q}, \infty) \\ &= (b_{inc})^2 \int d^3\vec{r} G_s(\vec{r}, \infty) \exp(i\vec{Q} \cdot \vec{r}) \equiv EISF(\vec{Q}), \end{aligned}$$

elastic incoherent structure factor

Recalling that self-correlation function, $G_s(\vec{r}, \infty)$, is the conditional probability density of finding a particle at \vec{r} and $t \rightarrow \infty$, given that the same particle was at $\vec{r}=0$ and $t=0$. Therefore, if a particle is confined in space indefinitely, $G_s(\vec{r}, \infty)$ has a finite value.

The \vec{Q} -dependence of a measured $EISF(\vec{Q})$ reveals the confinement volume.

The kinematical approximation

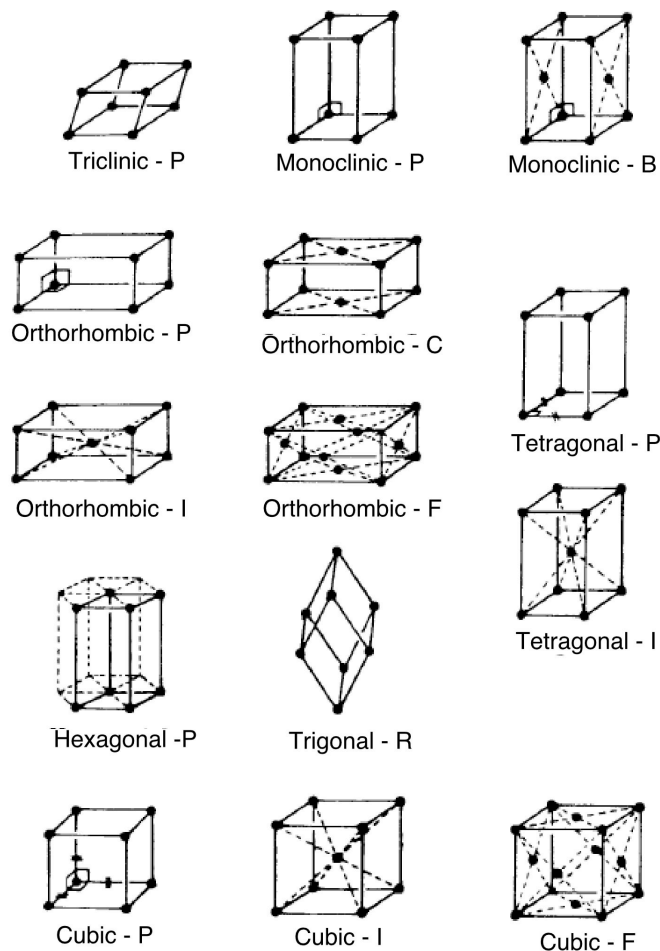
The *kinematical approximation* considers solely the single-scattering event of an incident beam of neutrons diffracted collectively by an assembly of atoms characterized by crystalline atomic planes, either in a perfect single crystal or an ideal powder, resulting in a coherently scattered beam captured by a detector (The Born Approximation). This approach does not take into account that neutron waves attenuate as they pass through a sample—the dynamical theory of diffraction. Some neutrons may consecutively be diffracted by multiple atomic planes, or some may be absorbed selectively by some of the atoms as they traverse the sample, resulting in attenuated secondary beams.

In the case of crystallography, if the size of a single crystal is small, typically not exceeding ~3 mm along any dimension, and the sample (single crystal or powder) does not contain substantial amounts of high neutron-absorptive elements, the kinematical approximation is by and large sufficient for the purpose of structural characterization. Major effects such as extinction and absorption are taken care of by empirical fudge factors in terms of adjustable parameters.

$Y(\lambda, \chi)$ a wavelength-dependent function to correct for extinction

$A(\lambda, \chi)$ a wavelength- and sample geometry-dependent function to correct for absorption

Incorporation of space-group symmetry is a must for crystallography



The conventional unit cells (thick black outline) of the 14 Bravais lattices.

Right: A typical starting page of a crystallographic space group in the International Table (top panel) and explanations of various entries (bottom panel).

$P 4/n$
No. 85
ORIGIN CHOICE 2

Origin at $\bar{1}$ on n , at $i, -i, 0$ from $\bar{4}$
Asymmetric unit $-i \leq x \leq i; -i \leq y \leq i; 0 \leq z \leq i$
Symmetry operations
(1) $\bar{1}$ 0,0,0 (2) 2 i, i, z $x, y, 0$ (3) 4^+ i, i, z $i, -i, z; i, -i, 0$ (4) 4^- i, i, z $-i, -i, z; -i, -i, 0$

C_{4h}^3
 $P 4/n$

$4/m$ Tetragonal
Patterson symmetry $P 4/m$

short International symbol serial number	Schönflies symbol full International symbol	point group International symbol	crystal system
ORIGIN CHOICE 2		Patterson symmetry	
			Obtained by placing glide planes by mirror planes and screw axes by rotation axes, and add an inversion center if the space group is not centrosymmetric. A Patterson symmetry represents a lattice symmetry that is consistent with inputting only the Bragg intensities (no phases).
	Space group diagram showing the location of symmetry operations in the unit cell. The upper left symbol denotes n-plane and m-plane.	Space group diagram showing the effect of symmetry operations applied on a circle at a general position in the outlined unit cell. Unit-cell convention: a-axis vertical pointing down, b-axis horizontal pointing right, and c-axis pointing up out of the paper.	
origin of the unit-cell coordinates (site symmetry)	Asymmetric unit A fraction of the unit cell that contains symmetrically inequivalent		
Symmetry operations	The symmetry operations of the space group each assigned a number. A numbered operation generates an equivalent position of the corresponding number given in the Coordinates table (below).		

International Tables for Crystallography, edited by Theo Hahn for the International Union of Crystallography (IUCr).

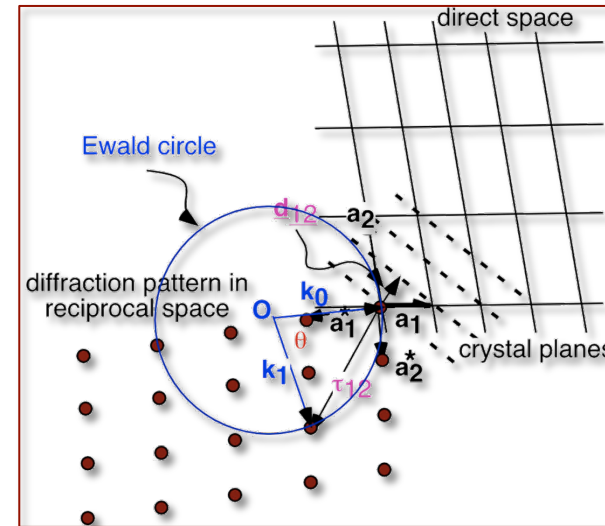
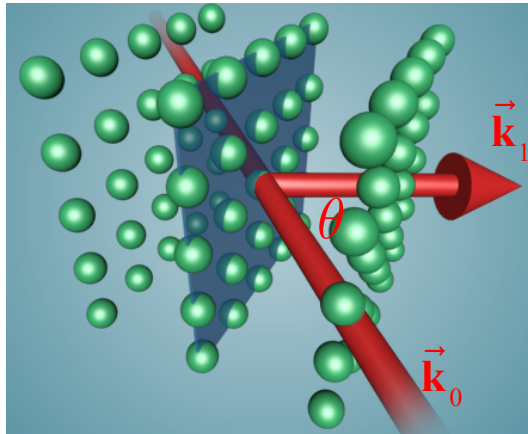
CONTINUED	No. 85	P 4/n
Generators selected (1); $r(1,0,0)$; $r(0,1,0)$; $r(0,0,1)$; (2); (3); (5)		
Positions		
Multiplicity, Wyckoff letter, Site symmetry	Coordinates	Reflection conditions
8 g 1	(1) x, y, z (5) $\bar{x}, \bar{y}, \bar{z}$	General: $hk0: h+k=2n$ $h00: h=2n$
	(2) $\bar{x}+\frac{1}{2}, \bar{y}+\frac{1}{2}, z$ (6) $x+\frac{1}{2}, y+\frac{1}{2}, \bar{z}$	Special: as above, plus
	(3) $\bar{y}+\frac{1}{2}, x, z$ (7) $y+\frac{1}{2}, \bar{x}, \bar{z}$	$hkl: h+k=2n$
	(4) $y, \bar{x}+\frac{1}{2}, z$ (8) $\bar{y}, x+\frac{1}{2}, \bar{z}$	$hkl: h, k=2n$
4 f 2..	i, i, z i, i, z i, i, z i, i, z	$hkl: h, k=2n$
4 e $\bar{1}$	$0, 0, \frac{1}{2}$ $i, i, \frac{1}{2}$ $i, 0, \frac{1}{2}$ $0, i, \frac{1}{2}$	$hkl: h, k=2n$
4 d $\bar{1}$	$0, 0, 0$ $i, i, 0$ $i, 0, 0$ $0, i, 0$	$hkl: h, k=2n$
2 c 4..	i, i, z i, i, z	no extra conditions
2 b $\bar{4}..$	$i, i, \frac{1}{2}$ $i, i, \frac{1}{2}$	$hkl: h+k=2n$
2 a $\bar{4}..$	$i, i, 0$ $i, i, 0$	$hkl: h+k=2n$
Symmetry of special projections		
Along [001] $p 4$ $a' = \frac{1}{2}(a-b)$ $b' = \frac{1}{2}(a+b)$ Origin at i, i, z	Along [100] $p 2mg$ $a' = b$ $b' = c$ Origin at $x, 0, 0$	Along [110] $p 2mn$ $a' = \frac{1}{2}(-a+b)$ $b' = c$ Origin at $x, x, 0$

CONTINUED	No. 85	P 4/n
Generators selected A set of symmetry operators chosen in such way that successively multiplying them will yield all the operators of the group.		
Positions		
Multiplicity, Wyckoff letter, Site symmetry	Coordinates	Reflection conditions
<p>At a general position, the no. of symmetry related positions is equal to the no. of symmetry operators of the point group unless centering increases the no. by a factor of n (n=1, 2, 4, 2, 3 for P, I, F, A, R respectively). For symmorphic space groups there is at least a '1' in column 1 where the point symmetry of that site is the same as that of the space group. For nonsymmorphic space groups no '1' but at least a '2'.</p> <p>The second column lists the Wyckoff designation of sites. In the third column the oriented site symmetries are given. Note that the position of the dot and the spaces carry special meanings. Under the Coordinates heading the coordinates of equivalent positions generated by symmetry operators for each site are given. The position numbers (within parentheses) for a general point correspond to the numbers of the generating symmetry operators.</p>		
Symmetry of special projections		
Projections of a 3-dimensional space group onto a plane will result in one of the 17 2-dimensional plane groups. Here such information is given for certain special projections.		
The presence of translational symmetry such as lattice centering, and glide-plane and screw-axis operations gives rise to systematic absences (extinction) of Bragg reflection intensities. Here the conditions for allowed reflections are given for each site.		

The continuing page of the P4/n crystallographic space group in the International Table (top panel) and explanations of various entries (bottom panel). Further listing of the subgroups and supergroups as well as the pages for a second choice of origin are omitted.

The Laue condition, Bragg's law and the Ewald sphere

$\vec{Q} \cdot \vec{R}_l = 2n\pi$ ($n = \text{an integer}$) for all \vec{R}_l , where \vec{R}_l is the position of the l^{th} site in a Bravais lattice.



An example of a crystallographic plane in the direct space and the occurrence of Bragg diffraction in the reciprocal space.

The elastic coherent scattering cross section is

$$\left(\frac{d\sigma}{d\Omega} \right)_{coh}^{el} = Nb_{coh}^2 \frac{(2\pi)^3}{v_0} \exp(-2W) \sum_{\vec{\tau}} \delta(\vec{Q} - \vec{\tau})$$

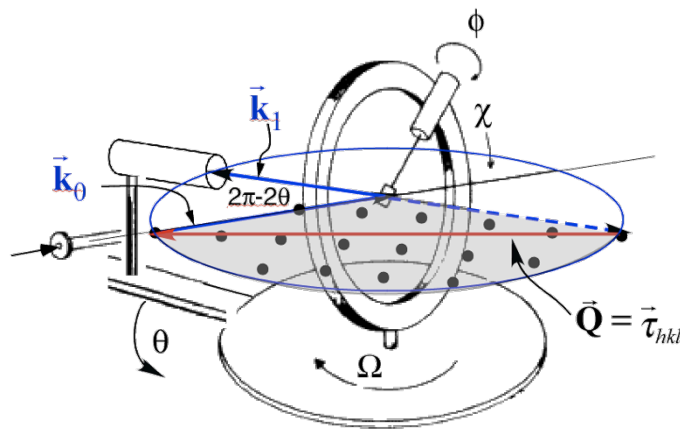
Therefore, diffraction from a perfect crystal yields non-zero intensities only at the reciprocal vectors characterized by hkl reflections. It can be seen from the fact of in the Debye-Waller factor that thermal motion of atoms suppresses the intensities, especially for the high-Q reflections. Wonder where the deducted intensities go? They reappear as thermal diffuse scattering (or phonons) in the inelastic region. The figure on the right illustrates the relation between the direct space of a crystallographic plane and corresponding diffraction pattern in the reciprocal space. The delta function implies that if coherent elastic scattering is to occur, $\vec{k}_0, \vec{k}_1, \vec{\tau}$ form an equilateral triangle with $\vec{\tau}$ being a reciprocal vector, i.e., connecting two reciprocal lattice points. Here the figure shows an example of $\vec{k}_0 - \vec{k}_1 = \vec{\tau}_{12}$.

Single-crystal diffraction

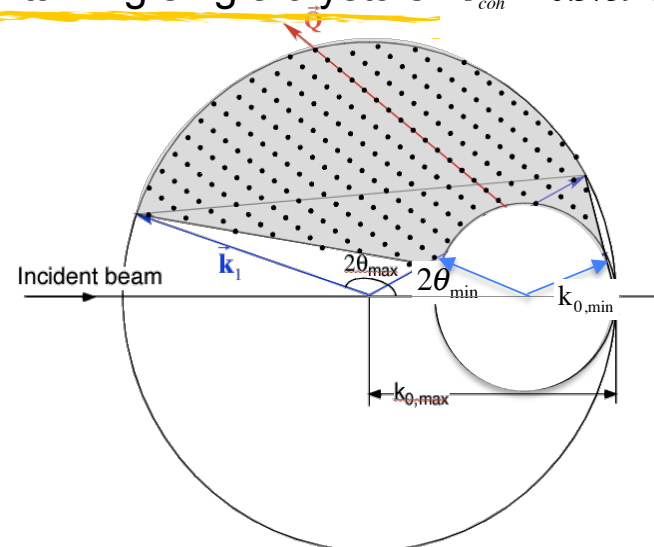
The crystallographic unit-cell structure factor is

$$F_{hkl} = \sum_i b_i \exp[2\pi i(hx_i + ky_i + lz_i)] \exp[-B_i(\sin \theta / \lambda)^2]$$

The detector is to measure the integrated intensity of a large number of Bragg reflections. Since the incident and scattered beams can be well collimated, signal-to-noise ratio is high. For example, it is possible to study hydrogen-containing single crystals. $b_{coh}^H = -0.3739 \times 10^{-12} \text{cm}$



Single-crystal diffraction with a monochromatic beam. Through sample rotation a set of the reciprocal lattice points is brought on to the scattering plane (shaded area). Bragg reflection occurs when the scattering wave vector \vec{Q} coincides with a reciprocal vector of hkl lattice planes, $\vec{\tau}_{hkl}$.



Time-of-flight single-crystal diffraction with the use of a polychromatic beam of which k_0 spans the range between $k_{0,\min}$ and $k_{0,\max}$. The reciprocal lattice points fixed by a chosen sample orientation are shown in two dimensions on the measurable region of the scattering plane (shaded) on which the detector angle varies from $2\theta_{\min}$ to $2\theta_{\max}$.

The time-of-flight Laue method

The Laue method employs a polychromatic neutron beam incident on the sample, i.e., the direction of \vec{k}_0 is fixed but its magnitude varies $k_0 \equiv k = \frac{2\pi}{\lambda}$. The incident flux of neutrons between λ and $\lambda + d\lambda$ is $\phi(\lambda)d\lambda$. For single crystals:

$$I_{Laue}^c = \int \phi(\lambda) \sigma_{coh}^{el} d\lambda$$

A detected spot may contain many reflections call the Laue orders

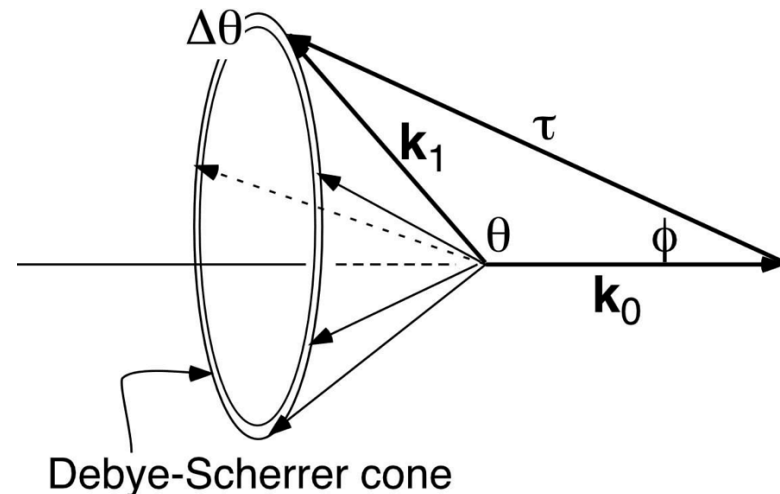
$$= N \frac{(2\pi)^3}{v_0} \frac{2}{k} |F_{hkl}(\vec{\tau})|^2 \int \phi(\lambda) \delta\left(\tau^2 - 2k\tau \sin\frac{\theta}{2}\right) \left(\frac{\pi}{k^2 \sin\frac{\theta}{2}} \frac{1}{\tau}\right) d\left(\tau^2 - 2k\tau \sin\frac{\theta}{2}\right)$$

$$= N \frac{(2\pi)^3}{v_0} \frac{2\phi(\lambda)}{k} |F_{hkl}(\vec{\tau})|^2 \left(\frac{\pi}{k^2 \sin\frac{\theta}{2}} \frac{1}{\tau}\right)_{\tau=2k \sin\frac{\theta}{2}}$$

$$= \frac{V\phi(\lambda)}{2v_0^2} \frac{\lambda^4}{\sin^2\frac{\theta}{2}} |F_{hkl}(\vec{\tau})|^2, \quad \text{the Lorentz factor}$$

The time-of-flight Laue method: By virtue of the time-of-flight technique on pulsed-source diffractometers, a series of Laue-order reflections manifests itself as separate peaks in the time domain along a fixed Bragg angle, thereby permitting the determination of a full data set. For powers:

$$I_{Laue}^p = \frac{V\phi(\lambda)}{4v_0^2} \frac{\lambda^4}{\sin^2\frac{\theta}{2}} j |F_{hkl}(\vec{\tau})|^2 \cos\frac{\theta}{2} \Delta\theta,$$



The monochromatic-beam method

For diffraction experiments at a steady-state source, a monochromatic beam of mean wavelength λ_0 with a width $\Delta\lambda_0$ is usually prepared. The incident flux is $\phi(\lambda_0)\Delta\lambda_0$. At a fixed angle the spread of wavelength of a diffracted beam, according to Bragg's law, is $\Delta\lambda_0 = \lambda_0 \cot\theta\Delta\theta$.

Powder

$$I_{\lambda_0}^p = \frac{V\phi(\lambda_0)\Delta\lambda_0}{4v_0^2} \frac{\lambda_0^3}{\sin\frac{\theta}{2}} j |F_{hkl}(\vec{\tau})|^2.$$

A detector is placed at the scattering angle 2θ for the reflection while the crystal is rotated about an axis perpendicular to the plane containing \vec{k}_0 and \vec{k}_1 .

Single Crystal

$$\begin{aligned} I_{\lambda_0}^c &= \frac{V\phi(\lambda_0)\Delta\lambda_0}{4v_0^2} \frac{\lambda_0^3}{\sin\frac{\theta}{2}} j |F_{hkl}(\vec{\tau})|^2 \left(\frac{\cos\frac{\theta}{2}\Delta\theta}{2} \right)^{-1} \\ &= \frac{V\phi(\lambda_0)\Delta\lambda_0}{v_0^2} \frac{\lambda_0^3}{\sin\theta} j |F_{hkl}(\vec{\tau})|^2 \frac{1}{\Delta\theta}. \end{aligned}$$

Rotating Single Crystal

$$\begin{aligned} I_{\lambda_0}^{rc} &= \frac{V\phi(\lambda_0)\Delta\lambda_0}{v_0^2} \frac{\lambda_0^3}{\sin\theta} j |F_{hkl}(\vec{\tau})|^2 \frac{1}{\Delta\theta} \frac{\Delta\theta}{2\pi} \\ &= \frac{V\phi(\lambda_0)\Delta\lambda_0}{v_0^2} \frac{\lambda_0^3}{2\pi \sin\theta} j |F_{hkl}(\vec{\tau})|^2. \end{aligned}$$

The Patterson function & Patterson symmetry

Let $f(\vec{r})$ be a continuous function of the atomic density of a crystal. In reality $f(\vec{r})$ consists of sharp peaks centered at the atomic positions of the unit cell, which is repeated to fill all space in three dimensions.

Patterson function defined as a convolution of $f(\vec{r})$ with itself, an autocorrelation function:

$$P(\vec{r}) \equiv \int_{-\infty}^{\infty} f^*(\vec{r}') f(\vec{r} + \vec{r}') d^3\vec{r}' = f^*(\vec{r}) \otimes f^*(-\vec{r}).$$

Therefore, the diffracted intensity is proportional to the Fourier transform of the Patterson function:

$$I^{el}(\vec{Q}) \sim \mathcal{F}[P(\vec{r})], \quad \text{and inversely,} \quad P(\vec{r}) \sim \mathcal{F}^{-1}[I^{el}(\vec{Q})].$$

We may generate a **Patterson map** in direct space using only the observed diffracted intensity. However, because of the lack of phase information, a Patterson map is NOT the real basic function. Rather, it contains *peaks that represent vectors between atoms but not the atoms themselves*. The symmetry of such a map is called the **Patterson symmetry**, and it is important to understand its differences from the crystallographic space group of the real structure.

Crystal structure refinement

For **single-crystal diffraction**, the observed and calculated structure factors (squared or modulus), $|F_{hkl}^X|^2$ or $|F_{hkl}^X|$, $X = obs$ or $calc$, are compared. The least-squares procedure is the process of minimizing the **weighted R-factors**, which provide measures of the goodness of the achieved structure solutions:

$$R_w(F^2) \equiv \left\{ \frac{\sum_{hkl} \left(\frac{1}{\sigma_{hkl}^2} \left(|F_{hkl}^{obs}|^2 - |F_{hkl}^{calc}|^2 \right)^2 \right)}{\sum_{hkl} \frac{1}{\sigma_{hkl}^2} \left(|F_{hkl}^{obs}|^2 \right)} \right\}^{1/2}, \quad \text{the weighted } R\text{-factor of } F^2;$$

σ_{hkl}^2 is an estimated statistical variance of $|F_{hkl}^{obs}|^2$

$$R_w(F) \equiv \left\{ \frac{\sum_{hkl} \left(\frac{1}{\sigma_{hkl}} \left(|F_{hkl}^{obs}| - |F_{hkl}^{calc}| \right) \right)^2}{\sum_{hkl} \frac{1}{\sigma_{hkl}} \left(|F_{hkl}^{obs}| \right)^2} \right\}^{1/2}, \quad \text{the weighted } R\text{-factor of } F.$$

For **powder diffraction** it is impractical to extract the integrated intensities of individual reflections due to peak overlapping at high Q. Instead, the entire observed diffraction profile is compared with the calculated one of a model structure. A least-squares fit that minimizes the difference between the two profiles

$$\chi^2 = \frac{1}{N - P} \sum_i w_i \left(Y_i^{obs} - Y_i^{calc} \right)^2$$

$$R_{wp} \equiv \left[\frac{\sum_i w_i \left| Y_i^{obs} - Y_i^{calc} \right|^2}{\sum_i w_i \left(Y_i^{obs} \right)^2} \right]^{1/2}, \quad \text{the weighted } R\text{-factor of the profile};$$

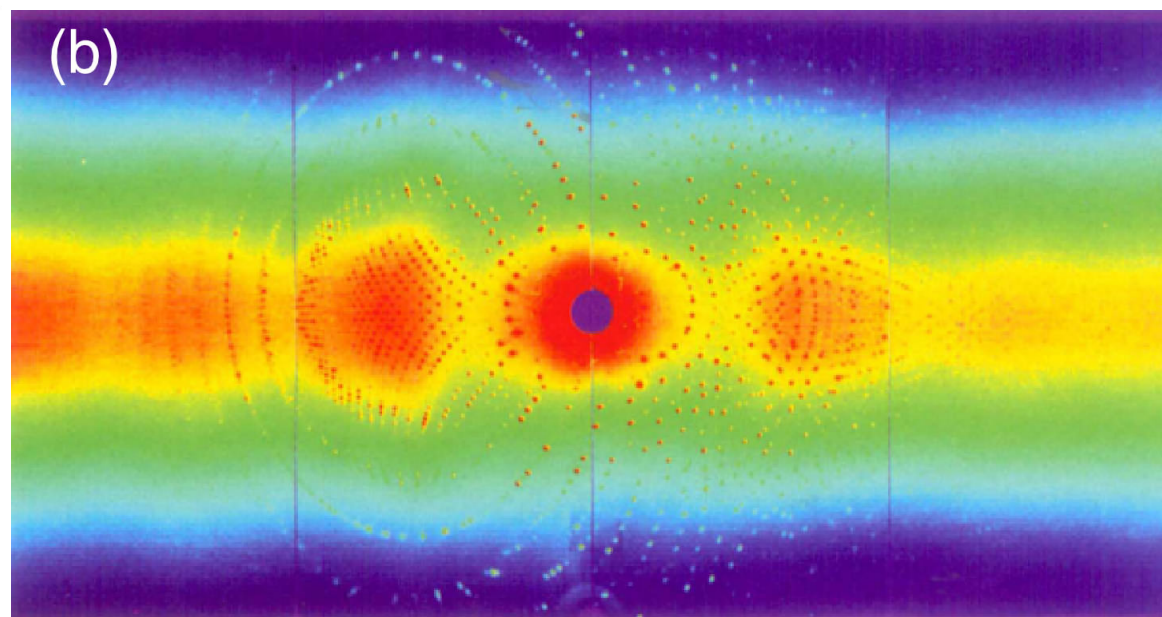
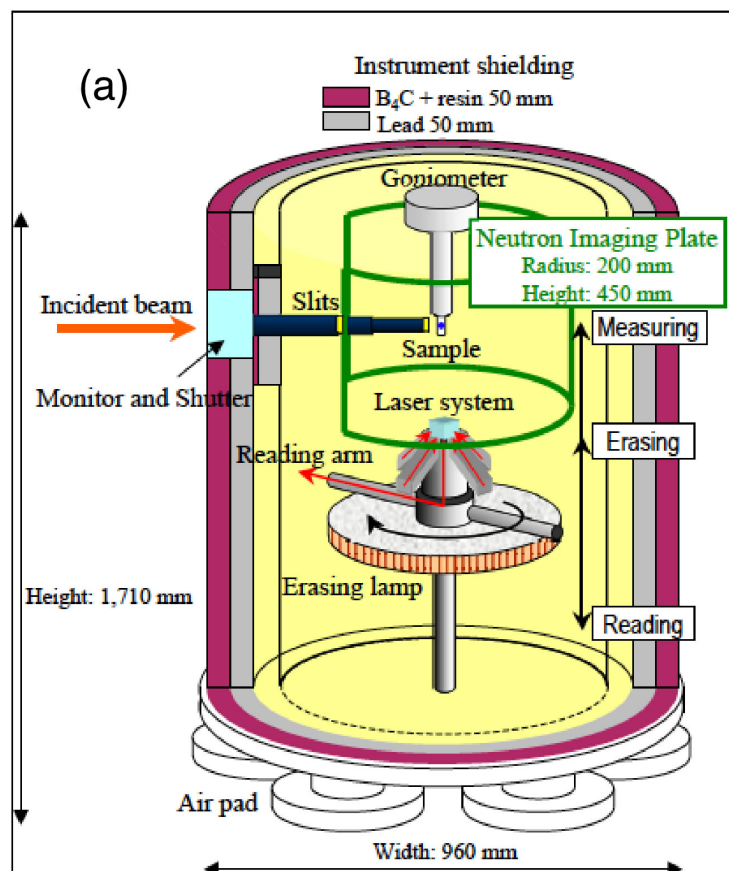
More practical details in GSAS tutorial (Antonella Scherillo)

Protein crystallography—neutrons vs x-rays

Today, most protein structures are investigated by x-ray diffraction at synchrotron radiation sources on account of the high brilliance of the photon fluxes and high instrumental resolution. However, the very limited and often incomplete information about the position of hydrogen atoms derivable from x-ray crystallography has hampered the understanding of important issues in biology such as protonation and hydration sites in proteins, water-substructures and hydrogen-bonding networks and pathways. Without such knowledge the structure-function relationship of biological macromolecules cannot be established. Neutrons, on the other hand, are sensitive to hydrogen; the opposite sign of the coherent scattering lengths of H and D permits contrast variation via *H/D exchange and labeling*. Furthermore, unlike x-rays, thermal neutrons do not inflict radiation damage on most biological substances and neutron experiments can be done at ambient temperature if necessary.

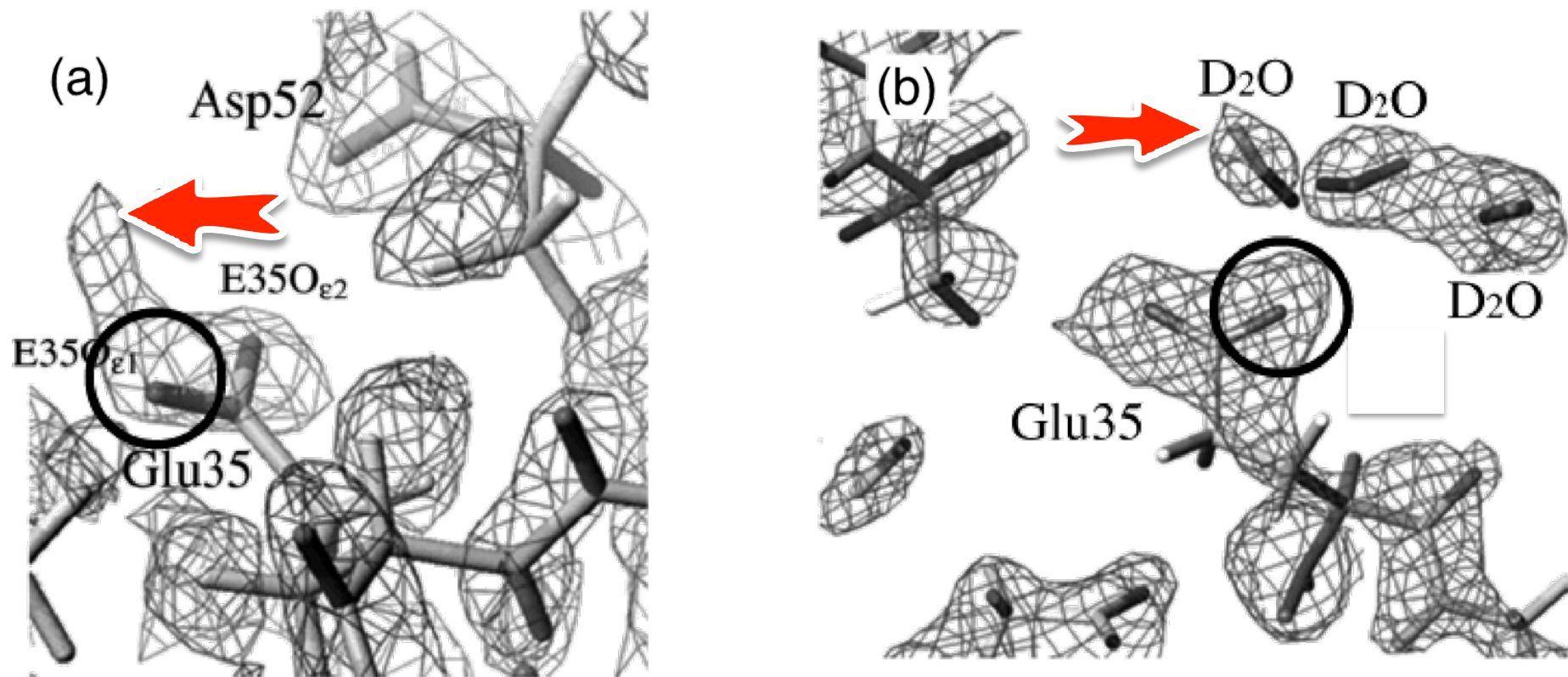
Neutron experiments are targeted to seek information on the whereabouts of *hydrogenous species in a crystal* whose basic structure is known other than hydrogen atoms from previous x-ray diffraction measurements.

Protein crystallography—The quasi-Laue method



(a) A schematic layout of the BIX-type of diffractometer that employs a quasi-Laue method for protein crystallography. The sequence of measuring, reading, and erasing data by the neutron image plate is automated for convenience and reproducibility. (b) An example of a recorded image, showing numerous spots of Bragg reflections for one setting of crystal orientation. The hole at the center permits the exit of the neutron beam. (Niimura et al. 1997 & 2007)

PD-dependent protonation sites in lysozyme



The nuclear density maps around the carboxyl group Glu35 of lysozyme at (a) $pD=4.9$ and (b) $pD=7.0$. In (a) the arrow points to a D atom connected to O atom (circled). But in (b) the protonation site disappears and the proton migrates to another site where it combines with a D atom to form a D₂O molecule. (Maeda et al. 2001 and Niimura et al. 1997)

Examples of diffraction experiments to illustrate:

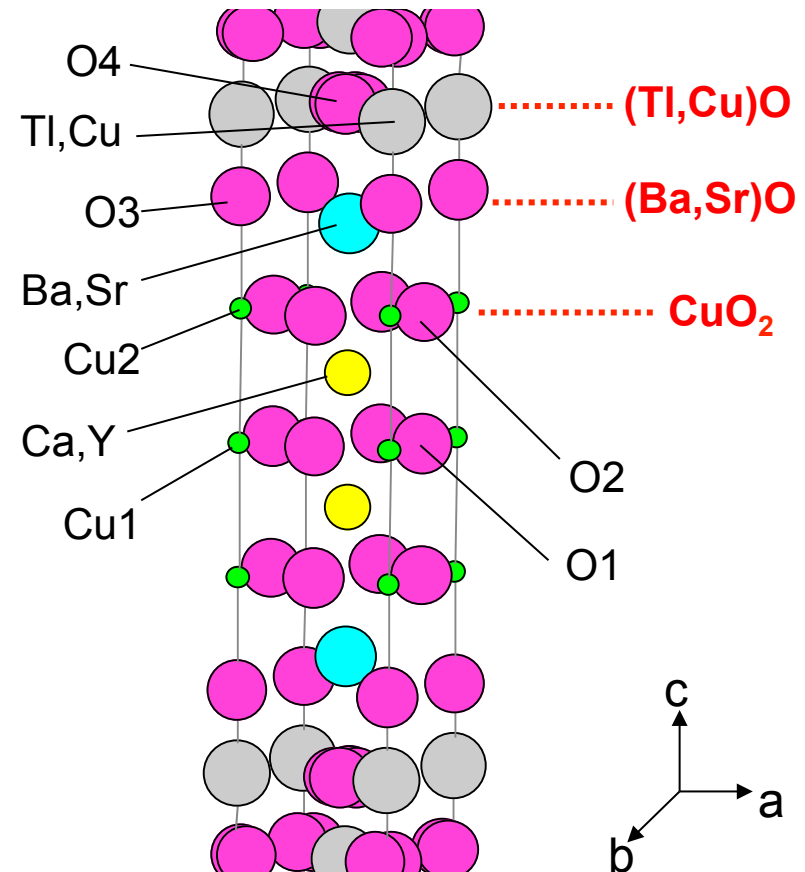
- ✧ Multifaceted scientific motivation
- ✧ Collaborative team efforts
- ✧ Complementary techniques
- ✧ The role of neutron study in the overall conclusions

$Tl_2(Ba_{1-x}Sr_x)_2Ca_2Cu_3O_y$ superconductors: Excess oxygen content & hole-carrying CuO_2 -layers

- ✧ $Tl_2(Ba_{1-x}Sr_x)_2Ca_2Cu_3O_y$ (Tl-2223) shows a T_c about 120K which is highest among the cuprate superconductors.
- ✧ Like other high- T_c cuprate superconductors, Tl-2223 exhibits the underlying layer structure that consists of CuO_2 planes separated by other M (metal cations) or MO layers parallel to the ab-plane.

Crystal chemistry concerning the excess oxygen content* and the CuO_2 -plane geometry is essential to understand the hole-conduction mechanism in the CuO_2 planes, hence the variation of T_c .

*Excess oxygen content $\Delta y = y - y_0 = O$ content calculated from the measured valence of Tl & Cu - O content assuming 3+ and 2+ for Tl and Cu, respectively



Complementary techniques & joint analyses

Approach:

Tokyo University of Science, Japan



- Carefully prepare TI-2223 polycrystalline samples with oxygen covering the underdoped-to-overdoped range.
- Measure the TI and Cu valence and T_c of all the samples.
- Measure the metal composition by chemical analysis.
- Calculate excess oxygen contents.
- Determine crystal structure and atomic positions especially for oxygen atoms.

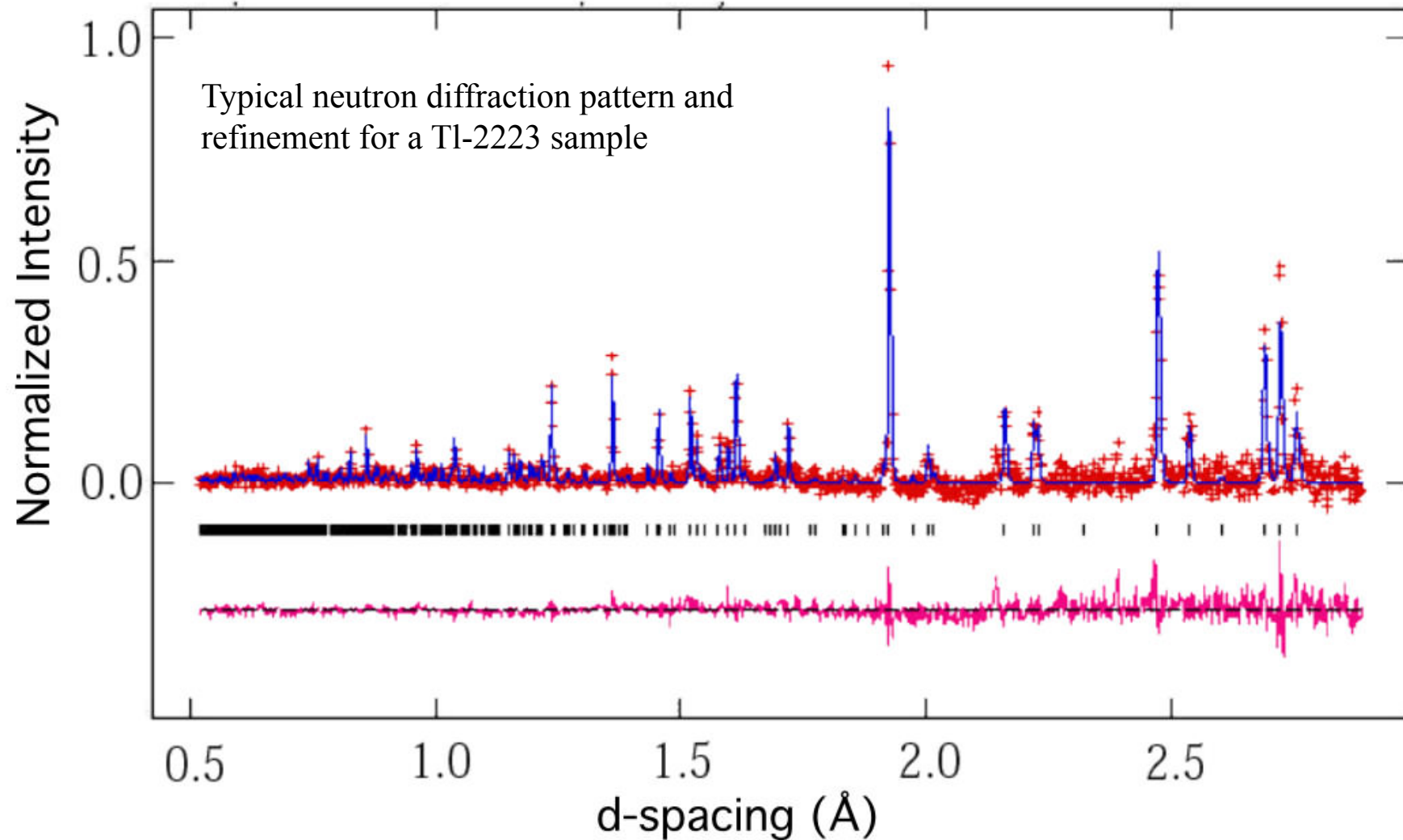
Methods: Redox titration with KBrO_3 , iodometry, four-probe DC method,

ICP, XRD & Neutron powder diffraction IPNS, Argonne, USA



Data analysis: Rietveld refinements of crystal structure, bond valence sum modeling

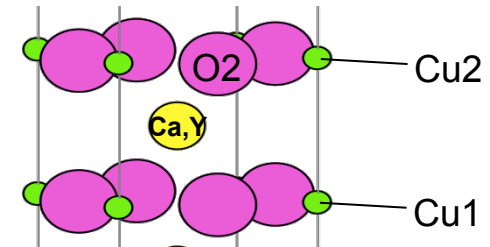
Correlation of crystal structure with optimal T_c and Δy



Space group $I4/mmm$; $a=0.385215(8)\text{nm}$ $c=3.56518(7)\text{nm}$ for
 $\text{Tl}_{1.8}\text{Ba}_{1.9}\text{Sr}_{0.1}\text{Ca}_{1.95}\text{Y}_{0.05}\text{Cu}_3\text{O}_{9.7}$

Correlation of crystal structure with Optimal T_c and Δy

- Relationship between lattice constants and TI content
- Trend of bond-length and bond-angle changes with respect to T_c
- Bond valence sums of Cu1 and Cu2

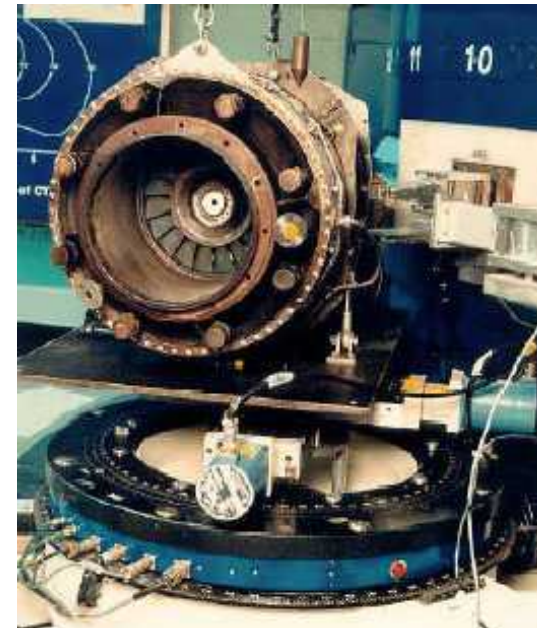
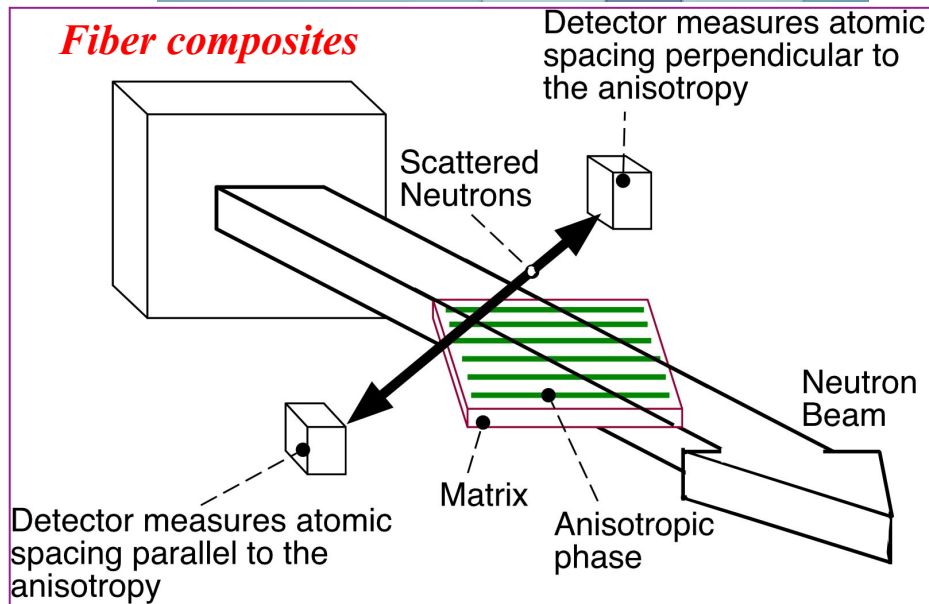
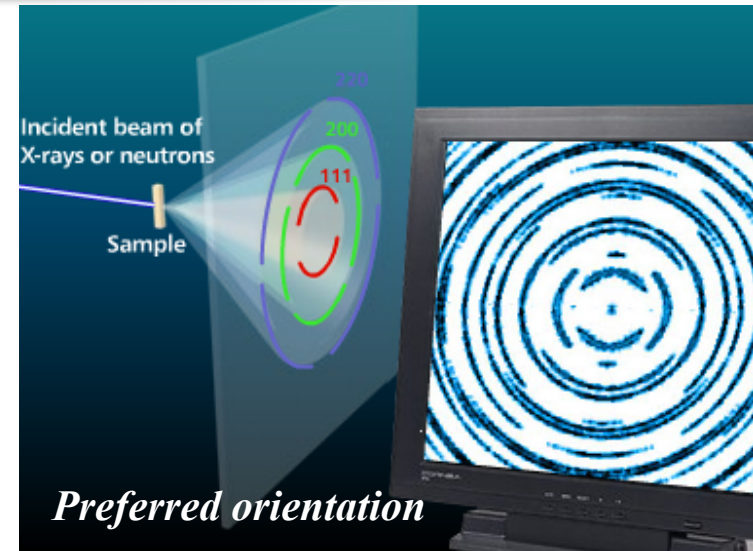
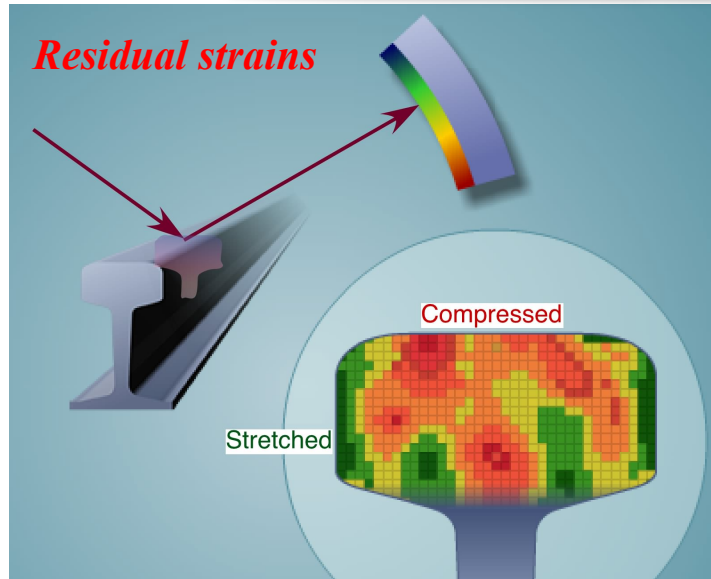


Conclusions

- Increasing bond angles connecting Cu2-O2-Cu2, O3-(Ba,Sr)-O3, & O4-Tl-O4 and/or decreasing Ca, Y site distortion lead to increase of T_c .
- From bond valence sum calculations, valence of Cu1 site is constant whereas valence of Cu2 site increases with increasing excess oxygen content. This implies **Cu2 site is responsible to the change of carrier concentration.**
- From crystal structural analysis, i.e., a **$\sim 176^\circ$ O2-Cu2-O2 bond angle**, **T_c shows maximum increase when a composition of TI-2223 induces (Cu2) O₂ plane close to an ideally flat geometry.** Similar trend was observed in YBCO and NCBCO superconductors from previous studies.

Idemoto, *et al.* (2004)

Neutron diffraction: Engineering applications



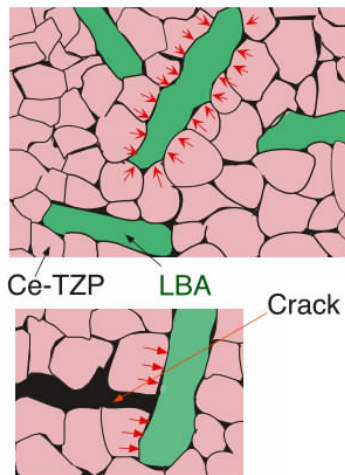
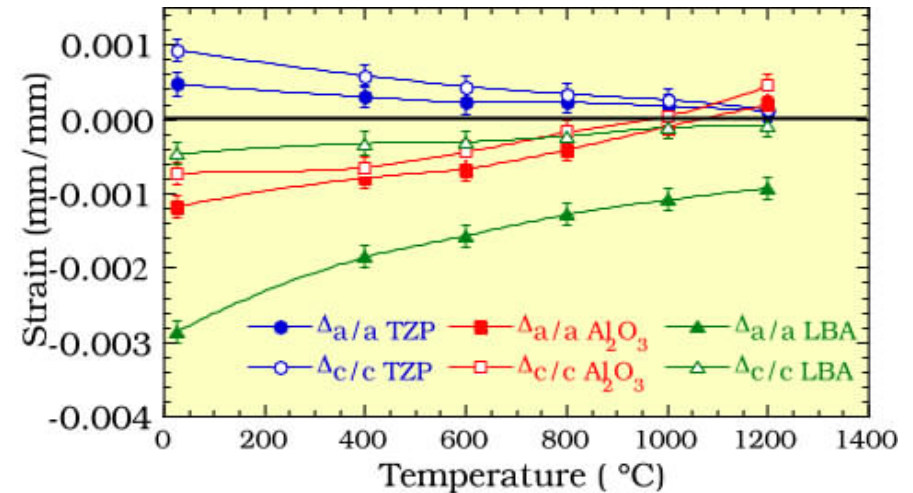
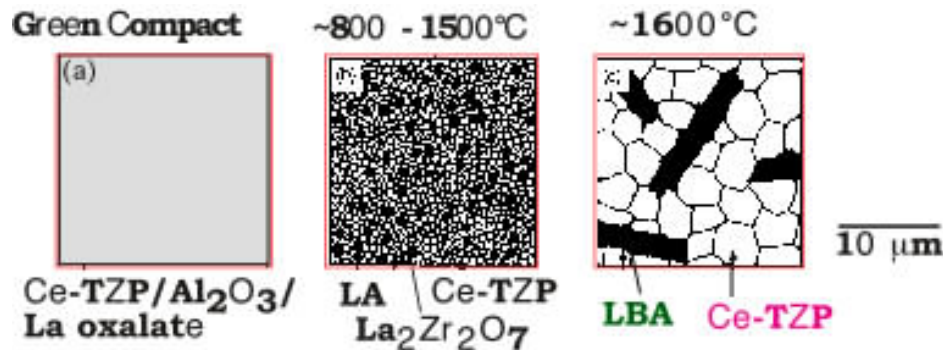
Ce-TZP/ Al_2O_3 /La- β -Aluminate composites

	Fracture strength (MPa)	Fracture toughness ($\text{MPa m}^{1/2}$)
Y-TZP	Degraded under low-temperature or hydrothermal ageing	
12Ce-TZP*	650	8.1
12Ce-TZP/ Al_2O_3 *	930	6.4
12CeTZP/Al_2O_3/LBA*	910	11.2

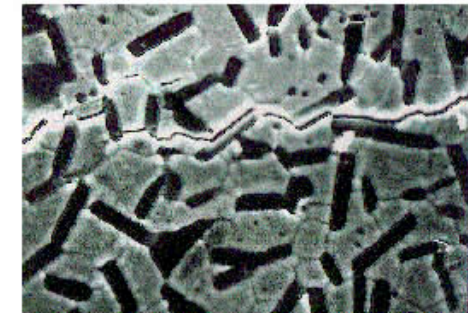
*Ce-TZP ~80wt%



T. Fujii, T. Kojima, W. Sakamoto, T. Yogo, S. Hirano
 Department of Applied Chemistry
 Nagoya University, Nagoya 464-01, Japan

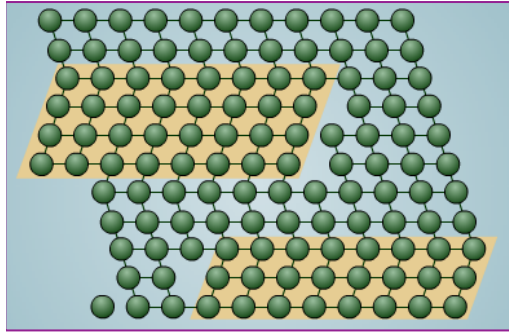


- The LBA crystals enforce ligamentary bridging of the Ce-TZP/ Al_2O_3 grains, blocking the crack-tip movement.
- The compressive residual stress on the crack walls exerts closure tractions to crack propagation.

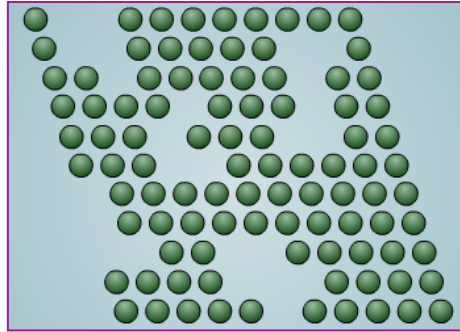


Not so perfect (long-range) ordering: Diffuse scattering

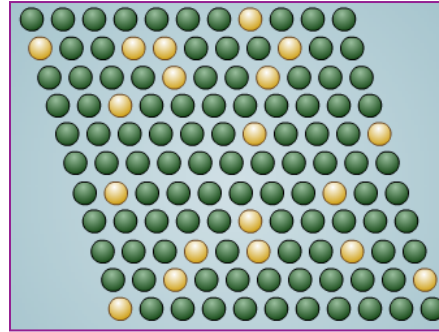
Stacking faults



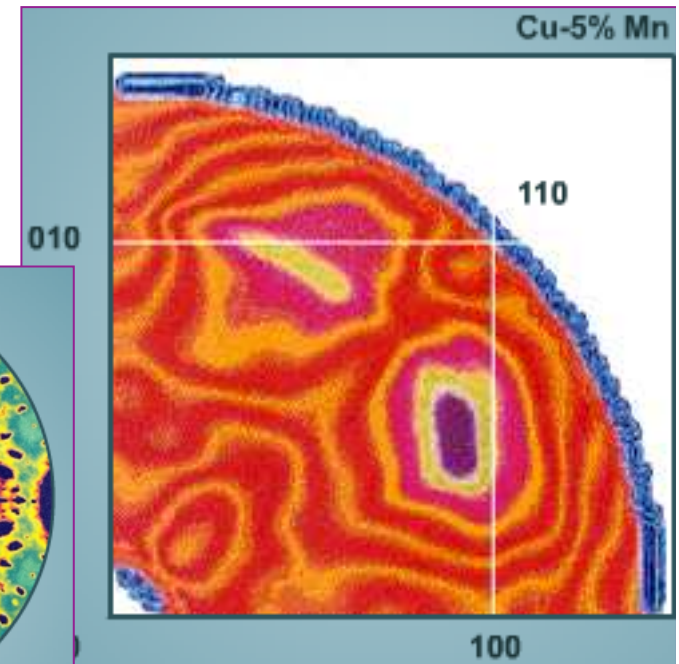
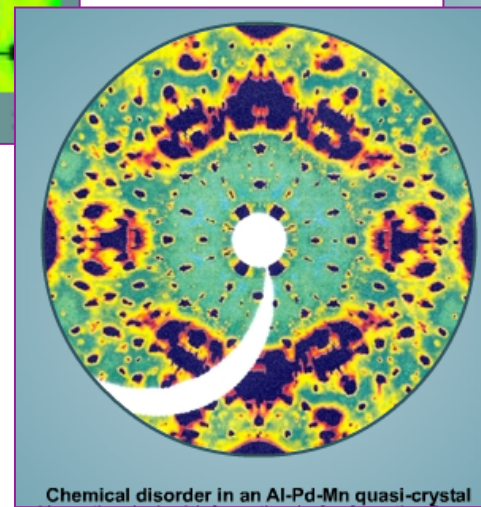
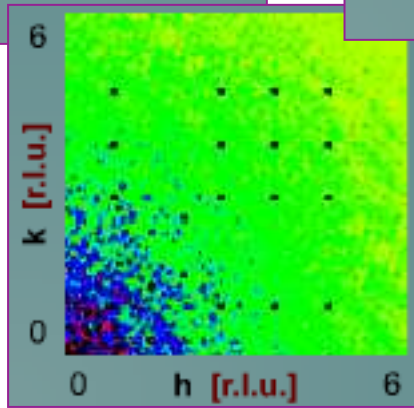
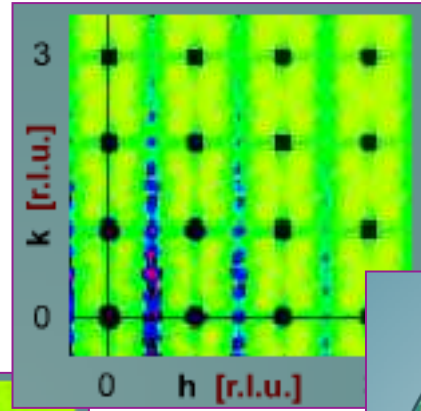
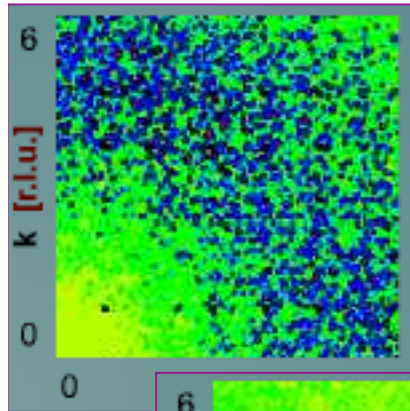
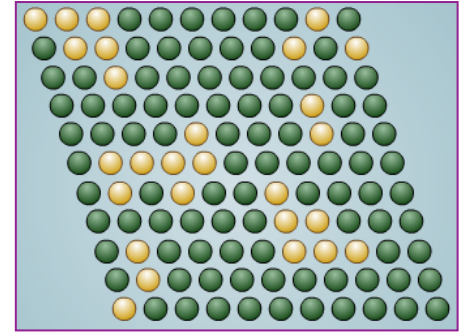
Vacancies



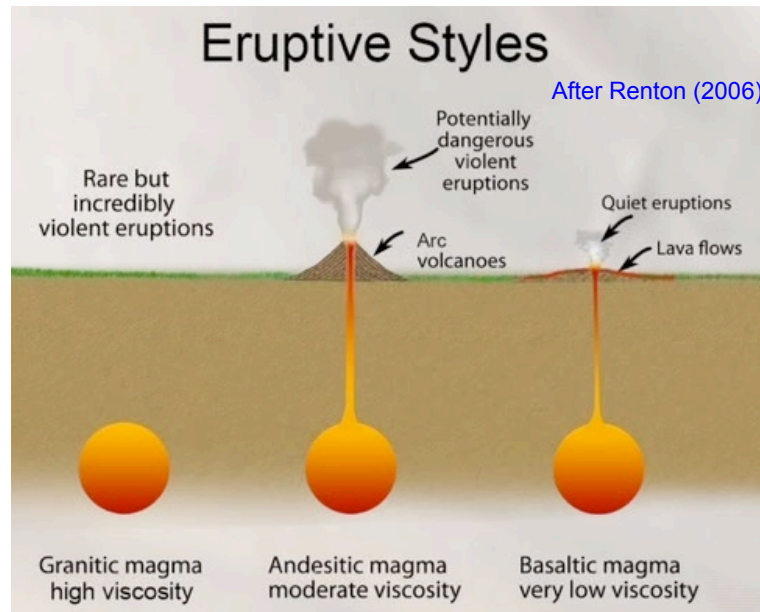
Impurities



Segregation



Why certain volcano eruptions are so violent & destructive but others not?



As occurring in Hawaii & Iceland today

Mt. Somma erupted ~10,000 years ago → Mt. Vesuvius erupted unexpectedly on Aug 24, 79 CE, destroying Herculaneum and Pompeii

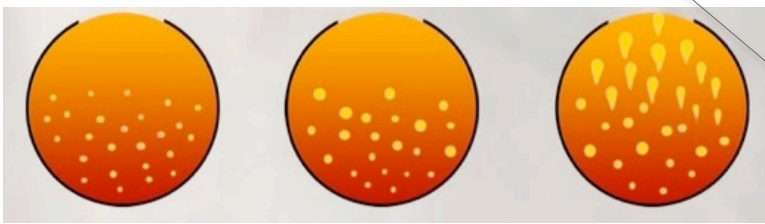


SiO₂ content

~45%

~55%

75-80%



gas bubbles form but are trapped behind the very viscous magma

gas bubbles get bigger and begin to develop buoyancy to compete with the viscous magma

gas bubbles grow to sufficient size and buoyancy to escape together with the running magma



Network connectivity at the limit: Vitreous forsterite $v\text{-Mg}_2\text{SiO}_4$




Silica glass ($v\text{-SiO}_2$) is perhaps the most studied inorganic glasses. The formation of a corner-sharing covalent network of SiO_4 tetrahedra makes the material—liquid, glassy and crystalline—very strong, chemically stable, having high melting point and high viscosity. Adding network modifying oxides such as NaO_x , BO_x , into silica substantially changes the thermodynamic properties of $v\text{-SiO}_2$, as seen in a variety of silicate glasses.

One of the most geological relevant minerals is forsterite, Mg_2SiO_4 . Its content of SiO_2 is considered as marginal in the formation of SiO_4 network hence understanding the liquid and glassy structures of forsterite are of utmost important..

But forsterite, the solid mineral widely found in the Earth's mantle, is always crystalline. How so we get around this problem to study vitreous forsterite, $v\text{-Mg}_2\text{SiO}_4$?

Vitreous Forsterite $v\text{-Mg}_2\text{SiO}_4$

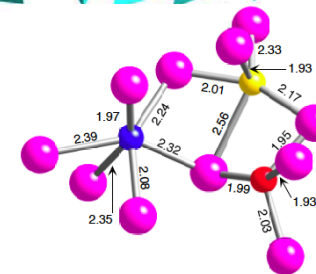
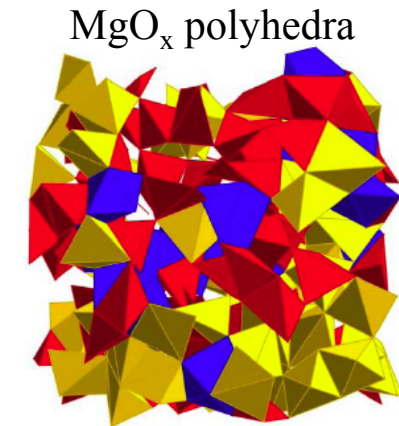
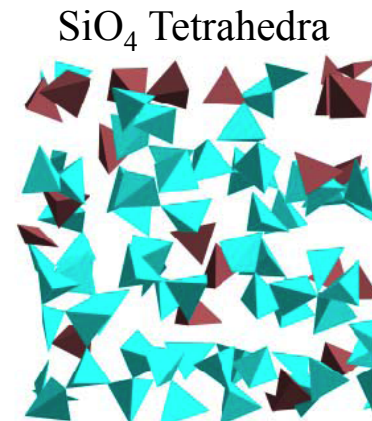
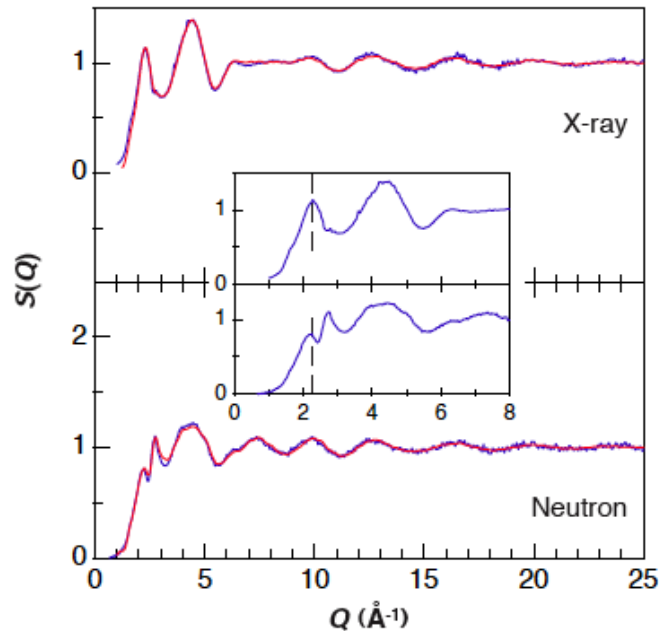
Approach:

- Synthesis of Mg_2SiO_4 glass by laser-melting containerless levitation - Containerless Research, Inc., USA 
- Synchrotron radiation x-ray diffraction - SPring8, Japan 
- Raman spectroscopy - Argonne, USA 
- Neutron Diffraction - IPNS, Argonne, USA
- Reverse Monte-Carlo simulations



$$S^X(Q) = 0.040 S_{\text{SiSi}}(Q) + 0.183 S_{\text{SiO}}(Q) + 0.137 S_{\text{SiMg}}(Q) + 0.209 S_{\text{OO}}(Q) + 0.313 S_{\text{OMg}}(Q) + 0.118 S_{\text{MgMg}}(Q)$$

$$S^N(Q) = 0.012 S_{\text{SiSi}}(Q) + 0.132 S_{\text{SiO}}(Q) + 0.061 S_{\text{SiMg}}(Q) + 0.371 S_{\text{OO}}(Q) + 0.344 S_{\text{OMg}}(Q) + 0.080 S_{\text{MgMg}}(Q)$$



● : 4 coordinated Mg,
 ● : 5 coordinated Mg
● : 6 coordinated Mg,
 ● : O

Kohara et al. (2004)

Network connectivity at the limit: Vitreous forsterite $v\text{-Mg}_2\text{SiO}_4$

Silica glass ($v\text{-SiO}_2$) is perhaps the most studied inorganic glasses. The formation of a corner-sharing covalent network of SiO_4 tetrahedra makes the material—liquid, glassy and crystalline—very strong, chemically stable, having high melting point and high viscosity. Adding network modifying oxides such as NaO_x , BO_x , into silica substantially changes the thermodynamic properties of $v\text{-SiO}_2$, as seen in a variety of silicate glasses.

One of the most geological relevant minerals is forsterite, Mg_2SiO_4 . Its content of SiO_2 is considered as marginal in the formation of SiO_4 network hence understanding the liquid and glassy structures of forsterite are of utmost important..

But forsterite, the solid mineral widely found in the Earth's crust, is always crystalline. How so we get around this problem to study vitreous forsterite, $v\text{-Mg}_2\text{SiO}_4$?

We found that the role of network former was largely taken on by corner and edge sharing of highly distorted, ionic Mg-O species that adopt 4-, 5-, and 6-coordination with oxygen. Future works are needed to extend the study of silicate minerals under the conditions of the Earth's mantle (under very high pressure and temperature) or in the interstellar environment.

References

Further reading

- Cowley, J. M. (1995). *Diffraction Physics*. Amsterdam: Elsevier Science B. V.
- Fultz, B., and Howe, J. (2008). *Transmission Electron Microscopy and Diffractometry of Materials*. Berlin: Springer-Verlag.
- Khidirov, I., Ed. (2012). *Neutron Diffraction*. Rijeka, Croatia: InTech.
- Pecharsky, V. K., and Zavalij, P. Y. (2009). *Fundamentals of Powder Diffraction and Structural Characterization of Materials*. New York: Springer Science.
- Robinson, K., and Tweet, D. J. (1992). Surface x-ray diffraction. *Rep. Prog. Phys.*, **55**, 599-651.

Useful papers

- Glazer, A. M. (1975), "Simple ways of determining Perovskite Structures." *Acta Crystallogr.* **A31**: 756-62.
- Niimura, N. (2012), "The pH dependence of protonation states of polar amino acid residues determined by neutron diffraction". in *Neutron Diffraction*. Ed., I. Khidirov. *Rijeka, Croatia*, InTech: 243-56.
- Niimura, N., Y. Minezaki, T. Nonaka, J.-C. Castagna, F. Cipriani, P. Høghøj, M. S. Lehmann and C. Wilkinson (1997), "Neutron Laue diffractometry with an imaging plate provides an effective data collection regime for neutron protein crystallography." *Nature Structural Biology* **4**(11): 909-14.
- Patterson, A. L. (1934), "A Fourier series method for the determination of the components of interatomic distances in crystals." *Phys. Rev.* **46**: 372-6.
- Patterson, A. L. (1935), "A direct method for the determination of the components of interatomic distances in crystals." *Z. Kristallogr.* **90**: 517-42.
- Rietveld, H. M. (1969), "A profile refinement method for nuclear and magnetic structures." *J. Appl. Crystallogr.* **2**: 65-71.
- Warren, B. E. (1941), "X-ray diffraction in random layer lattices." *Phys. Rev.* **59**(9): 693-8.